this text appeared in the proceedings of the ECMWF Seminar 2003 on
*Recent developments in data assimilation for atmosphere and ocean*

# Adaptive observations, the Hessian metric and singular vectors

**Martin Leutbecher**

*ECMWF, Shinfield Park, Reading*
*RG2 9AX, United Kingdom*

**ABSTRACT**

Techniques for planning adaptive observations that are based on tangent-linear models and their adjoints are discussed. The emphasis is on the validation of techniques that predict the statistically expected impact of additional non-routine observations on the forecast error. The concepts are illustrated using the Lorenz-95 system, which is a low-dimensional system that has similar error growth characteristics as operational NWP systems. The objective of a consistent approach to data assimilation and adaptive observations is formulated and illustrated for an extended Kalman filter and for an OI/3D-Var system. A reduced rank technique is introduced. It predicts forecast error variance in a singular vector subspace. The reduced rank predictions of forecast error variance are evaluated for both assimilation systems. Furthermore, a few examples are given of possible applications of the reduced rank estimate in the context of an operational variational assimilation scheme.

## 1 Introduction

Several techniques have been proposed that hold promise of identifying *optimal sites* for additional observations in order to improve numerical weather forecasts. Experience with such techniques has been and is going to be gained in field experiments as FASTEX, NORPEX, WSRP and the Atlantic TOST/TReC[1]. It has been documented for the past observation campaigns[2] that the use of targeted observations has overall a positive impact. However, we do not know how optimal the sites for the additional observations are really. So far, a proper[3] test to quantify the degree of optimality for the full NWP system is lacking because it would require a large number of additional observations: both targeted and un-targeted ones. The goal of this presentation is to advocate a more realistic target for targeted observation techniques: Can we predict how forecast uncertainty changes due to intermittent modifications of the observing network? Such predictions of changes of forecast uncertainty are necessarily part of any optimisation procedure for planning adaptive observations. A modification of the observing network will be called intermittent if it occurs only during an isolated assimilation cycle. Changes to the routine observing network that last over several subsequent assimilation cycles will not be covered here as they require appropriate techniques to account for the propagation of covariance information from one assimilation cycle to the next.

Predictions of changes of forecast uncertainty can be verified with observing system experiments in a similar way as the spread of ensemble forecasts is verified with the error of the ensemble mean or the error of the unperturbed control forecast. The equivalent of the spread-skill relationship for the adaptive observation problem is a change of forecast uncertainty – change of skill relationship. Such a kind of verification has been presented

[1] Fronts and Atlantic Storm-Track EXperiment (1997); The North Pacific Experiment (1998); Winter Storm Reconnaissance Program (1999-2003), THORPEX Observing System Test or THORPEX REgional Campaign (2003)

[2] About 10–40 dropsondes per case constituted the additional targeted observations in the past campaigns.

[3] that is with real observations, see e.g. Hansen and Smith (2000) or Leutbecher et al. (2002) for attempts to quantify optimality with observations taken from a simulated truth.

by Majumdar et al. (2001) for the Ensemble Transform Kalman filter technique (ETKF). The ETKF has been introduced by (Bishop et al. 2001) for observation targeting. The underlying assimilation scheme is computationally very efficient as it can work with subspaces of the dimension of the ensemble. The scheme belongs to the wider class of the Ensemble Square Root filters (Tippett et al. 2003). In their evaluation of the ETKF targeting approach, Majumdar et al. (2001) noted that the lack of consistency between the ETKF assimilation scheme on which the targeting is based and the operational 3D-Var used at NCEP to assimilate the additional dropsonde observations is a likely cause of discrepancies between the predicted reductions of forecast error variance and the actual realizations.

In order to predict changes of forecast uncertainty, knowledge is required about the statistics of initial condition errors, and of how they change due to the assimilation of additional observations, and about the perturbation dynamics from the assimilation time to the forecast verification time. All techniques that are currently feasible for operational NWP models assume either explicitly or implicitly that the perturbation dynamics can be approximated by a linear operator. Ensemble based techniques as the ETKF assume that linear combinations of ensemble perturbations are a solution of the model equations. For linear perturbation dynamics and Gaussian error statistics, optimal state estimation can be achieved with the extended Kalman filter. As outlined by Berliner et al. (1999) the extended Kalman filter is also the appropriate technique to objectively select optimal sites for additional observations. Current developments in data assimilation in general and in observation targeting in particular can be seen as an attempt to approximate the extended Kalman filter. Approximations of the extended Kalman filter are necessary due to the large dimension of the state space of NWP models. Several methods that aim at improving approximations of the extended Kalman filter can be found in these proceedings. One aim of this contribution is to explain and to verify approximate versions of the extended Kalman filter for observation targeting in the context of a low-dimensional system. Throughout this paper a perfect model scenario will be adopted, the contribution of model errors to forecast errors will be neglected.

Adjoint-based techniques such as sensitivity to initial conditions and singular vectors have been proposed to identify sensitive regions of the atmosphere in which additional observations should be taken (e.g. Palmer et al. 1998; Montani et al. 1999, and references therein). Two extensions of these techniques that actually account for the assimilation of additional observations are the Kalman filter sensitivity and the Hessian reduced rank estimate. The former, proposed by Bergot and Doerenbecher (2002), predicts forecast error variance in the direction of an adjoint sensitivity to the model state. The latter, introduced by Leutbecher (2003), predicts forecast error variance in the direction of a subspace of leading Hessian singular vectors. The Hessian reduced rank estimate can be seen as a special version of a more general class of singular vector based reduced rank techniques of predicting forecast error variance. We will start with the more general case. The method is explained and illustrated with the Lorenz-95 system, which may be one of the simplest dynamical systems that permits the construction of some nontrivial examples. Section 2 explains the methodology and section 3 contains the results. The Hessian reduced rank estimate in the context of an operational NWP framework is explained in section 4. The paper concludes with a discussion in section 5.

## 2 Adaptive observations in the Lorenz 95 system — Methodology

In his lecture at the 1995 predictability seminar at ECMWF, Edward Lorenz introduced a chaotic dynamical system that has similar error growth characteristics as operational NWP systems. I will refer to it from now on as L95. The L95-system is attractive as its dynamics are sufficiently complex and yet it is a low order system in which some advanced techniques can be tested easily. Therefore, the system is an ideal starting point for studies in data assimilation and predictability.

## 2.1 L95-dynamics

Here, we use a 40-variable version of the L95-system given by

$$\frac{dx_i}{dt} = -x_{i-2}x_{i-1} + x_{i-1}x_{i+1} - x_i + F, \tag{1}$$

where $i = 1, 2 \ldots 40$, and cyclic boundary conditions are used $x_0 = x_{40}$, $x_{-1} = x_{39}$, $x_{41} = x_1$. The magnitude of the forcing is set to $F = 8$. Lorenz (1995) concluded that similar error growth characteristics to operational NWP systems are obtained if a time unit in the L95-system is associated with 5 days. This scaling will be used throughout this paper. Solutions of the system are obtained by numerical integration with a fourth-order Runge-Kutta scheme using a 3-hour time-step ($\Delta t = 0.025$). For the chosen forcing, the system has 13 positive Lyapunov exponents, the largest corresponds to a doubling time of 2.1 days. The dynamics is the same for each variable as (1) is invariant under the transformation $i \rightarrow i+1$. Variables fluctuate about the mean in a non-periodic manner with a climatological standard deviation of $\sigma_{\text{clim}} = 3.6$. A perturbation of the initial condition will grow with time and its leading edge propagates "eastward" (to higher indices) at a speed of about 25 degrees/day. See Lorenz (1995) and Lorenz and Emanuel (1998) for a more detailed discussion of the system.

The system has been used previously for adaptive observation studies. Lorenz and Emanuel (1998) have compared various strategies for adding observations using a direct insertion data assimilation scheme. Berliner et al. (1999) have illustrated observation targeting based on the extended Kalman filter with the L95-system. Hansen and Smith (2000) compared the performance of various targeting strategies for both direct insertion and ensemble Kalman filter assimilation. They conclude that "for analysis errors of sufficiently small magnitude, dynamically based selection schemes will outperform those based only upon uncertainty estimates; it is in this limit that singular vector-based adaptive observation strategies will be productive."

## 2.2 Observing network

Now, the observing network is described that is used for the predictability experiments with the L95 system in this study. Observations become available every 6 hours. The observations are based on model states from a long integration of Eqn. (1) using the same setting as for the forecast model[4]. This integration is referred to as truth or truth run. Observed values are constructed by adding noise to the values taken from the truth run. The noise represents unbiased and uncorrelated normally distributed errors. The purpose is to mimic to some extent the inhomogeneous atmospheric observing network. Therefore, the 40-variables are divided into ocean points ($i = 1 - 20$) and land points (points $i = 21 - 40$, cf. Fig. 1). Over land, there is an observation at every location with a standard deviation of observation error of $0.05\,\sigma_{\text{clim}}$. Over the ocean, observations are available at "cloud-free locations" with an error standard deviation of $0.15\,\sigma_{\text{clim}}$. Clouds depend deterministically on the state $\mathbf{x}$ of the system but in such a way that the space-time pattern looks like a random process (Fig. 2). The probability for occurrence of cloud is 0.7. Land and ocean observations together constitute the *routine* observing network.

For the adaptive part of the observing network, a single additional observation with the error characteristics of a land observation is considered. The aim of adding this observation over the less well observed ocean is to improve the forecast at a chosen range of up to 5 days for the western part of the continent (sites 21–28), which will be referred to as "Europe" (Fig. 1). The evaluation of the targeting techniques is based on a 1000 day period during which additional observations (with $0.05\,\sigma_{\text{clim}}$) are available at every ocean site once daily[5].

[4] That means that a perfect model scenario is adopted.

[5] A major observing campaign also termed the **S**econd **H**emispheric **A**daptive observing, **P**redictability-**I**ntercomparison and **R**esearch **Ex**periment.

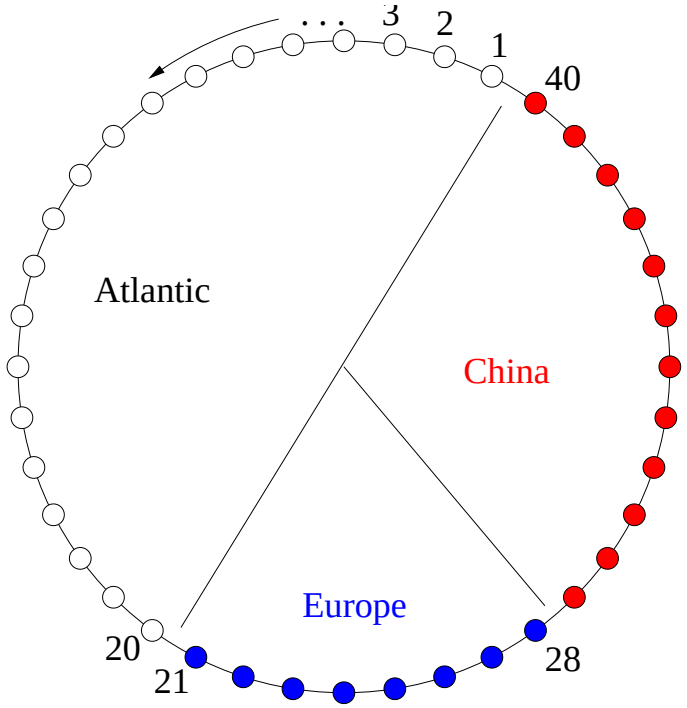


*Figure 1: The 1D-world of NWP in the L95-system*

Next, we will formulate the data assimilation and observation targeting methodologies that we will compare. We begin with an extended Kalman-filter in section 2.3. Section 2.4 deals with the reduced-rank approximation of the Kalman filter for the observation targeting part. Finally, a version of the reduced rank estimate that uses constant climatological background error covariances is introduced in section 2.5. Impact experiments use either none (control) or one of the additional observations and always start from the control-background fields and covariances.

### 2.3 Data assimilation and observation targeting with the extended Kalman filter

The covariance evolution in the Kalman filter is described by an alternating sequence of forecast steps and analysis updates. The covariance update can be written as

$$\left(\mathbf{P}_j^a\right)^{-1} = \left(\mathbf{P}_j^f\right)^{-1} + \mathbf{H}_j^{\mathrm{T}} \mathbf{R}_j^{-1} \mathbf{H}_j, \tag{2}$$

where the index $j$ denotes objects at time $t_j$. Otherwise, the notation follows the standard introduced by Ide et al. (1997). The covariance forecast from time $t_j$ to the next assimilation cycle at $t_{j+1}$ is given by

$$\mathbf{P}_{j+1}^f = \mathbf{M}_j(\Delta t)\, \mathbf{P}_j^a\, \mathbf{M}_j^{\mathrm{T}}(\Delta t) + \mathbf{Q}, \tag{3}$$

where $\mathbf{M}_j(\Delta t)$ denotes the propagator of the tangent-linear model from time $t_j$ to time $t_{j+1} = t_j + \Delta t$. It is necessary to include a small model error term $\mathbf{Q}$ in order to avoid filter divergence. The nonlinear model is perfect but the linear model used in the extended Kalman filter is imperfect due to linearisation errors[6].

[6]The model error covariance matrix is represented with a diagonal matrix with $q_{kk} = 5 \times 10^{-3} \sigma_{\mathrm{clim}}$ for ocean points and $q_{kk} = 5 \times 10^{-4} \sigma_{\mathrm{clim}}$ for land points. At the western seaboard there is a smooth transition of $q$ from ocean values to land values to account for the eastward advection of larger errors.

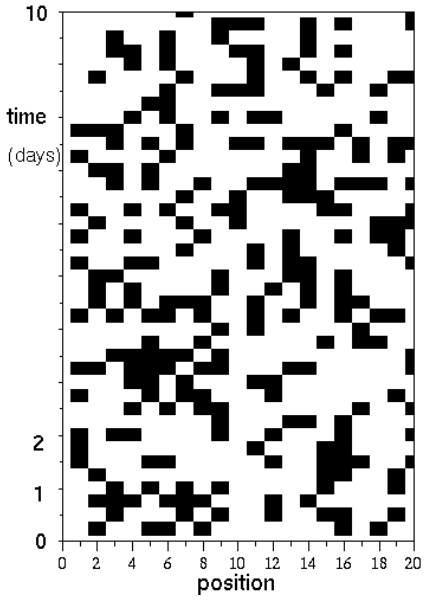


*Figure 2: Hovmuller diagram of cloud cover (white) affecting the data coverage of observations over the ocean (sites 1–20)*

The application of the Kalman filter to observation targeting requires an extension of the forecast range and variance localisation. The linear prediction of the forecast error variance in the verification region at time $t_{j+\ell} = t_j + \ell\Delta t$ is then given by the trace of

$$\mathbf{L}_{\mathrm{Eu}}\mathbf{P}^f_{j+\ell}\mathbf{L}^{\mathrm{T}}_{\mathrm{Eu}} = \mathbf{L}_{\mathrm{Eu}}\mathbf{M}_j(\ell\Delta t)\,\mathbf{P}^a_j\,\mathbf{M}^{\mathrm{T}}_j(\ell\Delta t)\mathbf{L}^{\mathrm{T}}_{\mathrm{Eu}}, \tag{4}$$

where the contribution of the model error term $\mathbf{Q}$ has been neglected. The operator $\mathbf{L}_{\mathrm{Eu}}$ denotes the projection operator for the verification region ($(\mathbf{L}_{\mathrm{Eu}})_{jj} = 1$ for $j = 21, 22, \ldots, 28$ and 0 otherwise).

The prediction of changes of forecast error variance in the verification region due to an additional observation at location $i$ proceeds similarly. From now onwards, there is no need to refer to different assimilation cycles. Therefore, the time index $j$ is dropped. New indices $r$ and $i$ are introduced to refer to the routine observing network and an additional observation at location $i$, respectively. Index $i$ is used in two ways: The 40-by-1 and 1-by-1 matrices $\mathbf{H}_i, \mathbf{R}_i$ refer to observation operator and error variance "matrix" for the additional observation at location $i$ whereas the symbols $\mathbf{P}^a_i, \mathbf{P}^f_i$ denote the covariance matrices for the routine observing network augmented by the additional observation at site $i$. The effect of the additional observation on the analysis error covariance matrix valid at time $t_j$ is described by

$$(\mathbf{P}^a_i)^{-1} = \left(\mathbf{P}^f_r\right)^{-1} + \mathbf{H}^{\mathrm{T}}_r\mathbf{R}^{-1}_r\mathbf{H}_r + \mathbf{H}^{\mathrm{T}}_i\mathbf{R}^{-1}_i\mathbf{H}_i = (\mathbf{P}^a_r)^{-1} + \mathbf{H}^{\mathrm{T}}_i\mathbf{R}^{-1}_i\mathbf{H}_i \tag{5}$$

Note, that the covariance update (5) starts from the routine forecast error covariance matrix $\mathbf{P}^f_r$ valid at time $t_j$. This is consistent with the assumption that the modification of the observing network is isolated in time. The covariance matrix is evolved from $t_j$ to $t_{j+\ell}$ via

$$\mathbf{P}^f_i = \mathbf{M}\,\mathbf{P}^a_i\,\mathbf{M}^{\mathrm{T}}, \tag{6}$$

where $\mathbf{M}$ denotes the propagator from $t_j$ to $t_{j+\ell}$. The reduction of forecast error variance in the verification region that is due to an additional observation at position $i$ is then given by

$$r_i = \mathrm{trace}\left(\mathbf{L}_{\mathrm{Eu}}\left(\mathbf{P}^f_r - \mathbf{P}^f_i\right)\mathbf{L}^{\mathrm{T}}_{\mathrm{Eu}}\right). \tag{7}$$

The optimal position for an adaptive observation is the one that maximises (7).

## 2.4 A reduced rank approximation of the covariance forecast step in the Kalman filter

Approximations to the Kalman filter are important in order to develop techniques that are feasible for current NWP models with state space dimensions ranging from $10^5$ to $10^7$. In this section, we explore an approximation to the covariance forecast step (Eqn. 3). for the prediction used for planning the adaptive observations. For the assimilation of data, an extended Kalman filter is used as in the previous section. The approximation reduces the rank of the problem by predicting the variance of forecast errors only in a subspace of leading singular vectors. Formally, this means that trace$(\mathbf{L}_{\mathrm{Eu}}\mathbf{P}^f\mathbf{L}_{\mathrm{Eu}}^{\mathrm{T}})$ is replaced by trace$(\Pi_n\mathbf{L}_{\mathrm{Eu}}\mathbf{P}^f\mathbf{L}_{\mathrm{Eu}}^{\mathrm{T}}\Pi_n^{\mathrm{T}})$, where $\Pi_n$ denotes a projection into the $n$-dimensional subspace of leading singular vectors of $\mathbf{L}_{\mathrm{Eu}}\mathbf{M}$. The singular vectors are computed with the inverse of the routine analysis error covariance matrix $(\mathbf{P}_r^a)^{-1}$ as initial time metric because these singular vectors evolve into the leading eigenvectors of the forecast error covariance matrix $\mathbf{L}_{\mathrm{Eu}}\mathbf{P}_r^f\mathbf{L}_{\mathrm{Eu}}^{\mathrm{T}}$. We will use the notation $\mathbf{V}_n = (\mathbf{v}_1 \ldots \mathbf{v}_n)$ for the matrix containing the leading $n$ initial singular vectors as columns.

For the routine observing network, the analysis error covariances in the singular vector subspace can be represented by $\mathbf{V}_n\mathbf{V}_n^{\mathrm{T}}$ because the singular vectors $\mathbf{v}_j$ are orthonormal with respect to the routine analysis error covariance metric $(\mathbf{P}_r^a)^{-1}$. Intuitively, it makes sense that only initial errors in the direction of the initial singular vectors need to be accounted for if one is interested in the forecast error in the direction of the evolved singular vectors. A formal proof is given in Leutbecher (2003). For the augmented observing network, the analysis error covariances are represented by an outer product of transformed singular vectors $\mathbf{V}_n\Gamma_i\Gamma_i^{\mathrm{T}}\mathbf{V}_n^{\mathrm{T}}$. The $n$-by-$n$ transformation matrix $\Gamma_i$ is an inverse square root of the matrix

$$\mathbf{C}_i = \mathbf{V}_n^{\mathrm{T}}(\mathbf{P}_i^a)^{-1}\mathbf{V}_n = \mathbf{I}_n + \mathbf{V}_n^{\mathrm{T}}\mathbf{H}_i^{\mathrm{T}}\mathbf{R}_i^{-1}\mathbf{H}_i\mathbf{V}_n. \tag{8}$$

The matrix $\mathbf{C}_i$ is the modified analysis error covariance metric expressed in the basis of the singular vectors. This representation of the analysis error covariances involves an approximation of the full covariance matrix by a block-diagonal form — see Leutbecher (2003) for further details. Using these representations of the analysis error covariances, the forecast error variance in the verification region turns out to be

$$\mathrm{trace}(\Pi_n\mathbf{L}_{\mathrm{Eu}}\mathbf{P}^f\mathbf{L}_{\mathrm{Eu}}^{\mathrm{T}}\Pi_n^{\mathrm{T}}) = \begin{cases} \sum_{j=1}^{n}\sigma_j^2 & \text{for the routine network and} \\ \mathrm{trace}(\Gamma^T\mathrm{diag}(\sigma_1^2,\ldots,\sigma_n^2)\Gamma) & \text{for the modified network.} \end{cases} \tag{9}$$

Here, $\sigma_j$ denotes the singular value of singular vector $\mathbf{v}_j$.

## 2.5 Approximation using a reduced rank covariance prediction and a climatological background error covariance matrix

The next step of approximating the full Kalman filter is the replacement of the predicted forecast error covariance matrix $\mathbf{P}^f$ in the assimilation by a static matrix $\mathbf{B}$ (Eqn. 2). This approximation will be used consistently for the data assimilation part and the targeting part. Subsequently, we will refer to it as the OI-assimilation scheme[7]. Variational assimilation schemes can be viewed as implementations of the Kalman filter that are initialised with a fixed static background error covariance matrix $\mathbf{B}$ at the initial time of each assimilation cycle. With this approximation of the background error covariances, the analysis error covariance matrix is given by

$$\mathbf{A}^{-1} = \mathbf{B}^{-1} + \mathbf{H}^{\mathrm{T}}\mathbf{R}^{-1}\mathbf{H}. \tag{10}$$

[7] OI-schemes for NWP applications also select observations. This aspect is not considered here.

| range (d) | 0 | 1 | 2 | 3 | 4 | 5 |
|---|---|---|---|---|---|---|
| KF | 0.11 | 0.17 | 0.25 | 0.38 | 0.57 | 0.80 |
| OI | 0.33 | 0.49 | 0.74 | 1.04 | 1.38 | 1.74 |

$\sigma_{\text{clim}} = 3.6, \quad \sigma_{o,\text{land}} = 0.18, \quad \sigma_{o,\text{ocean}} = 0.54$

*Table 1: Kalman filter (KF) versus optimum interpolation (OI) performance, global rms errors*

For the L95-system, the background error matrix has been obtained from forecast-minus-truth[8] differences from the 1000-day period[9]. The diagnosed estimate $\mathbf{B}^{(n)}$ depends on the estimate $\mathbf{B}^{(n-1)}$ used in the assimilation. Superscripts refer to the iteration number. The iterations are started with a diagonal matrix $\mathbf{B}^{(0)}$. A few iterations are required until the estimate of the background error covariance matrix converges. The approximation of the background error covariances is combined with the reduced rank technique introduced in the previous section: Forecast error variances are predicted in a subspace of leading singular vectors. The motivation for this twofold approximation is that it leads to a system that is similar to the current implementation of the Hessian reduced rank estimate for the ECMWF forecasting system. The latter will be discussed in section 4.

# 3 Adaptive observations in the Lorenz 95 system — Results

Now, we turn to the verification of the variance predictions obtained with the three different targeting techniques. Results are based on a 1000-day period. There are 21 different forecasts on each day: The control forecast and the 20 forecasts using an additional observation at site $i$, $i = 1, \ldots, 20$. The latter always start from the control forecast as background. The results obtained with the Kalman filter will be compared with the results obtained with the two reduced rank approximations. Due to the low dimensionality of the system, we will consider only the rank 1 version of the reduced rank approximations. At the end of the section, the impact of the additional targeted observations will be discussed.

## 3.1 Skill of forecast systems using the routine observations

Before discussing results of the observation targeting experiments, it is of interest to compare the skill of the forecast system using an OI assimilation scheme with that of the forecast system using a Kalman filter assimilation scheme. Global rms errors of analyses and forecasts are given in Tab. 1. The Kalman filter analyses and short-range forecasts are about three times more accurate than the optimum interpolation analyses and forecasts. The 1-day forecast error of the Kalman filter system is about as large as the observation error of a land observation and the 1-day forecast error of the optimum interpolation system is similar to the error of an ocean observation.

## 3.2 Prediction of forecast error variance reductions

The goal of targeting techniques — as advocated throughout this paper — is to make skilful predictions of how forecast error variance is reduced due to various upgrades of the observing system. A prerequisite for this is the prediction of forecast error variances. Forecast error variance prediction is one of the classical aims of

[8] truth is defined in section 2.2.

[9] This technique should provide an upper bound on forecast errors for all techniques using a static representation of **B** because truth is unknown and further approximations of **B** are required for operational NWP systems. See Mike Fisher's contribution for a description of how **B** is estimated and represented in operational NWP systems.

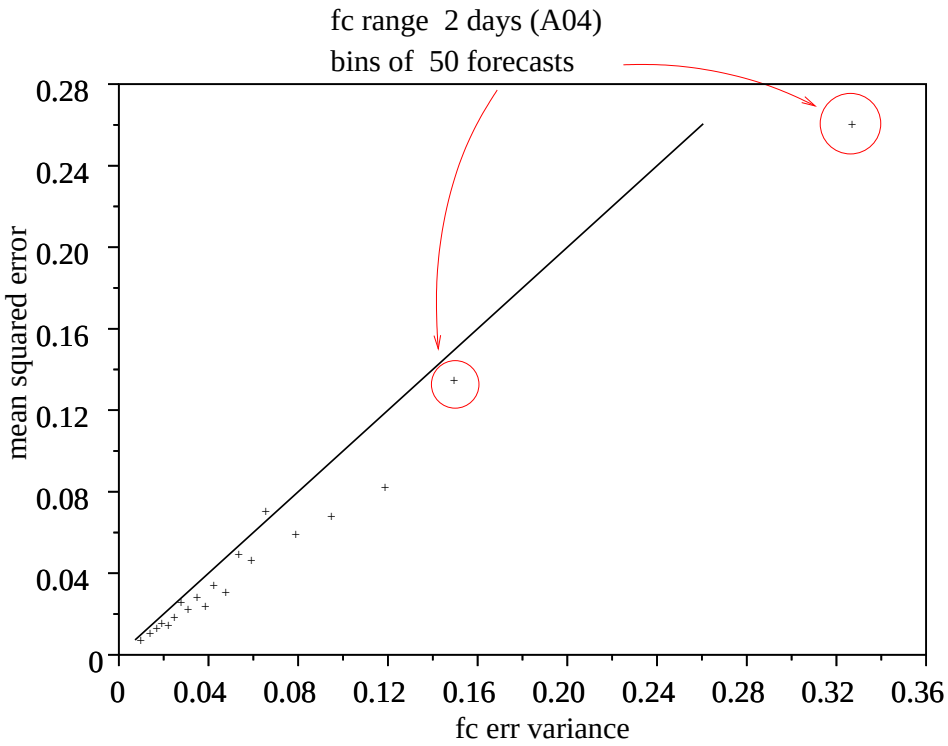


*Figure 3: Mean squared error versus Kalman filter variance predictions. 2 day forecast range, verification region "Europe". Size of bins...*

ensemble prediction. The corresponding verification diagrams are referred to as spread-skill diagrams. In the linear regime, there is no need for a Monte-Carlo approach. In the Kalman filter, the variances are evolved explicitly using the tangent-linear model via (4). Figure 3 shows the verification of this variance prediction for the 2-day forecast for Europe for the system that uses the routine observations only. Cases are stratified with the predicted 2-day forecast error variance in the verification region and grouped into bins of 50 forecasts each in order to construct the diagram. The mean predicted variance in each bin is plotted on the abscissa whereas the mean squared error in each bin is plotted on the ordinate. The latter constitutes asample estimate of the actual variance. For a perfect system, all points will scatter close to the diagonal. The scatter around the diagonal will decrease with increasing bin size. There appears to be a tendency for slightly too large variance predictions. This may be due to a conservative estimate of the model error term in the Kalman filer and due to nonlinear error saturation effects.

Now, we turn to the predictions of forecast error variance *reductions*. We begin with the (full rank) Kalman filter and then turn to the two levels of approximation in subsequent sections.

### 3.2.1 Kalman filter predictions

The predictions of forecast error variance reductions in the full rank Kalman filter are based on Eqn. (7). The verification of these predictions proceeds similarly to the verification of the variance predictions themselves. Cases are now stratified by the predicted reduction of forecast error variance. Figure 4 shows the verification for the 2-day forecast over "Europe" for bin sizes of 50 and 250. The number of bins in Fig. 4a is larger than in Fig. 3 because there are now 20 realizations of a variance reduction each day. However, as the background

error is the same in these realizations the data are not independent. In consequence the relationship between predicted and realized reductions in forecast error variance is still quite noisy for a bin size of 50. The scatter is considerably reduced at a bin size of 250. There is a small tendency to over-predict forecast error reductions. Apart from this minor discrepancy, the Kalman filter based prediction of forecast error variance reductions is skilful. We note that large sample sizes may be required for the verification.

#### 3.2.2 Kalman filter-rank-1 predictions

Now, we turn to the verification of the approximate version of the Kalman filter targeting that uses rank reduction based on a subspace of leading singular vectors. Only the rank 1 case is considered here. The reduction of the total mean square error in the verification region is compared with the predicted reduction of forecast error variance in the subspace of the leading singular vector. The verification for forecast day 2 is plotted in Fig. 5. The rank-1 predictions of variance reduction are of a similar magnitude as the full-rank predictions. The projection of forecast errors in the direction of the leading singular vector will result in smaller variances for every forecast: the one using the routine observations and each one using an augmented observing network. However, the block-diagonal approximation of the analysis error covariance matrix for the modified observing network results in an underestimation of the associated forecast error variance. The net effect is a moderate over-prediction of forecast error variance reductions. This appears plausible as the forecast error explained by the leading singular vector is quite large in this low dimensional system.

#### 3.2.3 OI-rank-1 predictions

Next, we verify forecast error variance reductions obtained with the rank-1 system that uses climatological background error covariances. From the perspective of current NWP applications, this is the most interesting step as the similar systems can be designed for operational NWP systems. The Hessian reduced rank estimate, which will be discussed in section 4, is one example. Predicted and actual reductions of forecast error variance in the L95-system are compared in Fig. 6. The average realized mean square error reductions increase monotonically with the predicted rank 1 error variance reductions. Generally, the OI-rank 1 system significantly over-predicts the variance reductions. This feature could be removed by an empirical scaling of the predicted variance reductions.

The different performance of the optimum interpolation system (OI) and the Kalman filter system (KF) has two causes: the different covariance estimate and the different accuracy of the trajectory upon which the linearisation is based. As mentioned previously, the trajectory of the OI-system has about a three times larger error than the trajectory of the KF-system. In order to disentangle the two causes one can compare with Kalman filter results for longer forecast ranges. The 4-day error of the KF-system has a similar magnitude as the 2-day error in the OI-system (Tab. 1). The verification of forecast error variance reductions is plotted in Fig. 7. We notice a useful monotonically increasing relationship. There is evidence for nonlinear error saturation effects for predicted reductions of forecast error variance larger than 1 but no sign of saturation for reductions smaller than 0.5. In the OI-system, the overestimation of variance reductions is independent of the predicted reduction. This suggests that the constant background error covariance estimate is the main cause for the systematic overestimation of variance reductions in the OI-system.

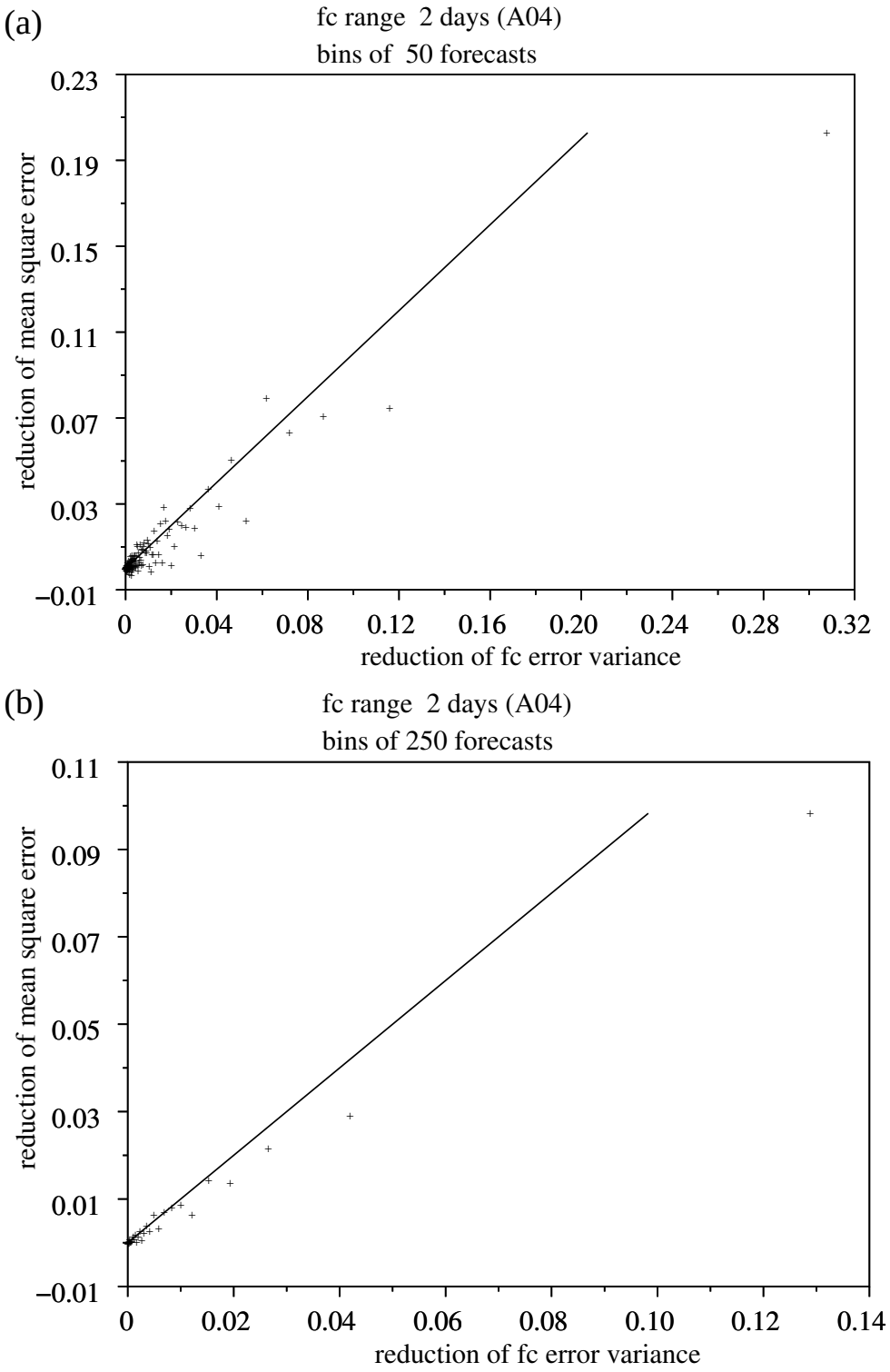


*Figure 4: Verification of the predictions of forecast error variance reductions due to additional observations (Kalman filter). Top panel: bins of 50 forecasts; bottom panel: bins of 250 forecasts*

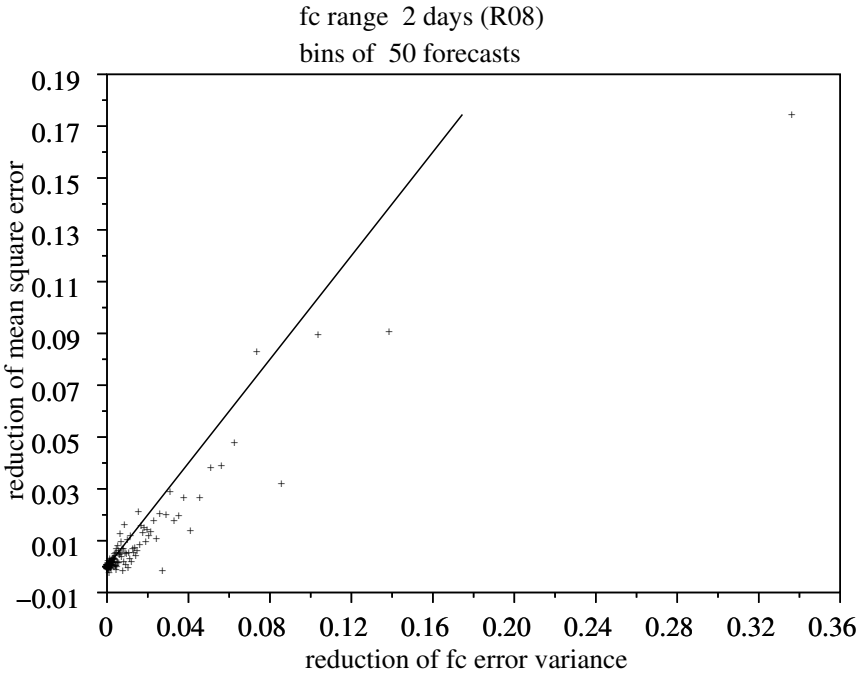


*Figure 5: Evaluation of the Kalman Filter rank-1 predictions of forecast error variance reductions due to additional observations. 2-day forecast and bins of 50 forecasts.*

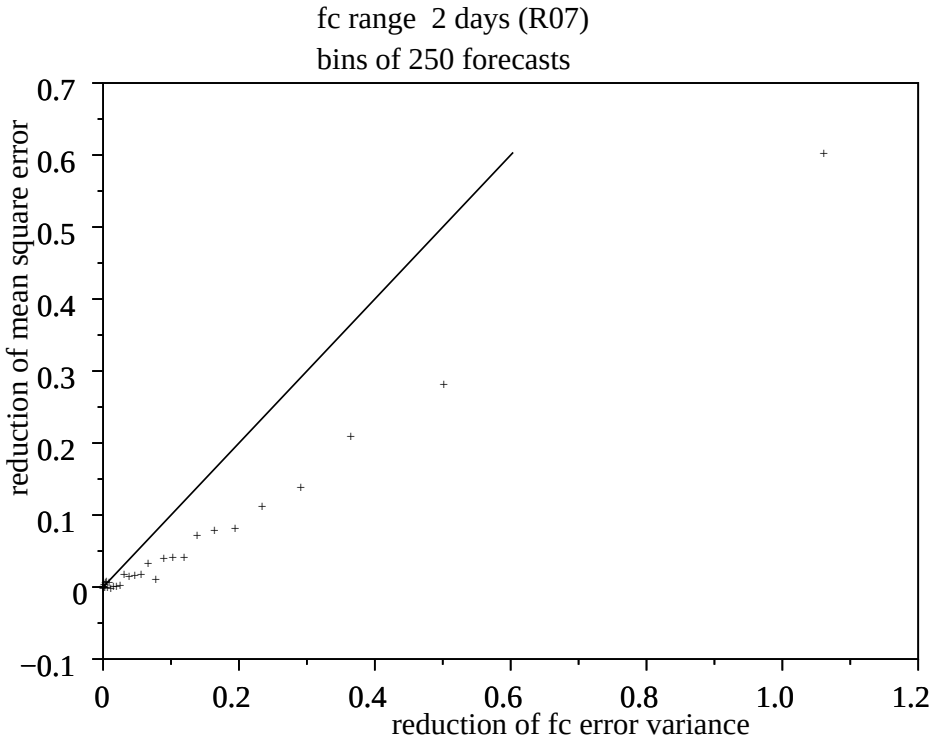


*Figure 6: Verification of 2-day forecast error variance reductions: OI-rank 1. 2-day forecast and bins of 250 forecasts.*

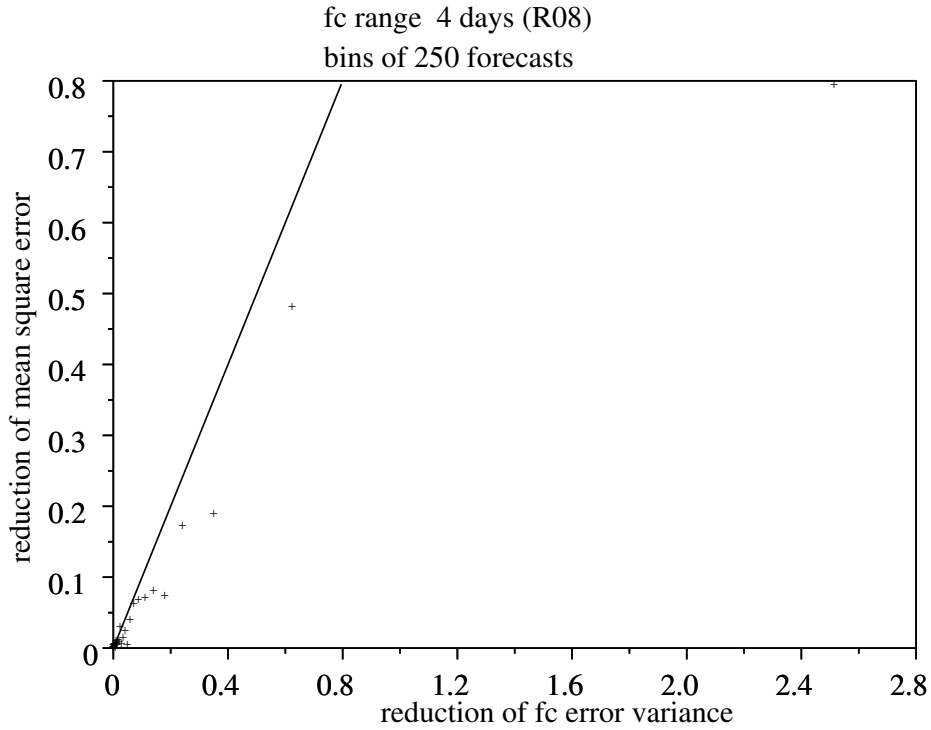


*Figure 7: Verification of Kalman filter rank-1 predictions of forecast error variance reductions due to additional observations. 4-day forecast and bins of 250 forecasts.*

### 3.3 Impact of adaptive observations on the forecast error distribution

Figure 8 illustrates the fact that the optimal site for an additional observation depends on the underlying assimilation scheme. Next, we look at the impact that the adaptive observation has on the distribution of forecast errors (Fig. 9). A hard test for any targeting scheme that adapts positions for additional observations on a daily basis is whether it outperforms a scheme that adds an observation at the best fixed site. Based on Fig. 8, site 19 and 20 are selected as best[10] fixed sites for the KF and OI-system, respectively. For both systems, the forecasts using targeted observations are significantly better than the forecasts using the fixed additional observation or the forecast using routine observations only. Further, we note that the rank-1 KF targeting and full-rank KF-targeting yield almost identical reductions of the forecast error distribution. The forecast improvement obtained with an additional observation at a fixed site in the OI-system is fairly small compared to the improvement obtained with the rank-1 OI targeting. Note, that observation targeting is particularly efficient in reducing the risk for particularly large forecast errors, say the largest 5–10% of errors.

## 4 Reduced rank prediction of forecast error variance reductions in an operational NWP context

The reduced rank methodology for predicting the effect of additional observations on forecast uncertainty has been introduced in the context of a low-dimensional system in section 2. Now, we will see how this idea can be

[10] Another choice would be the site that actually leads to the largest forecast error reduction.

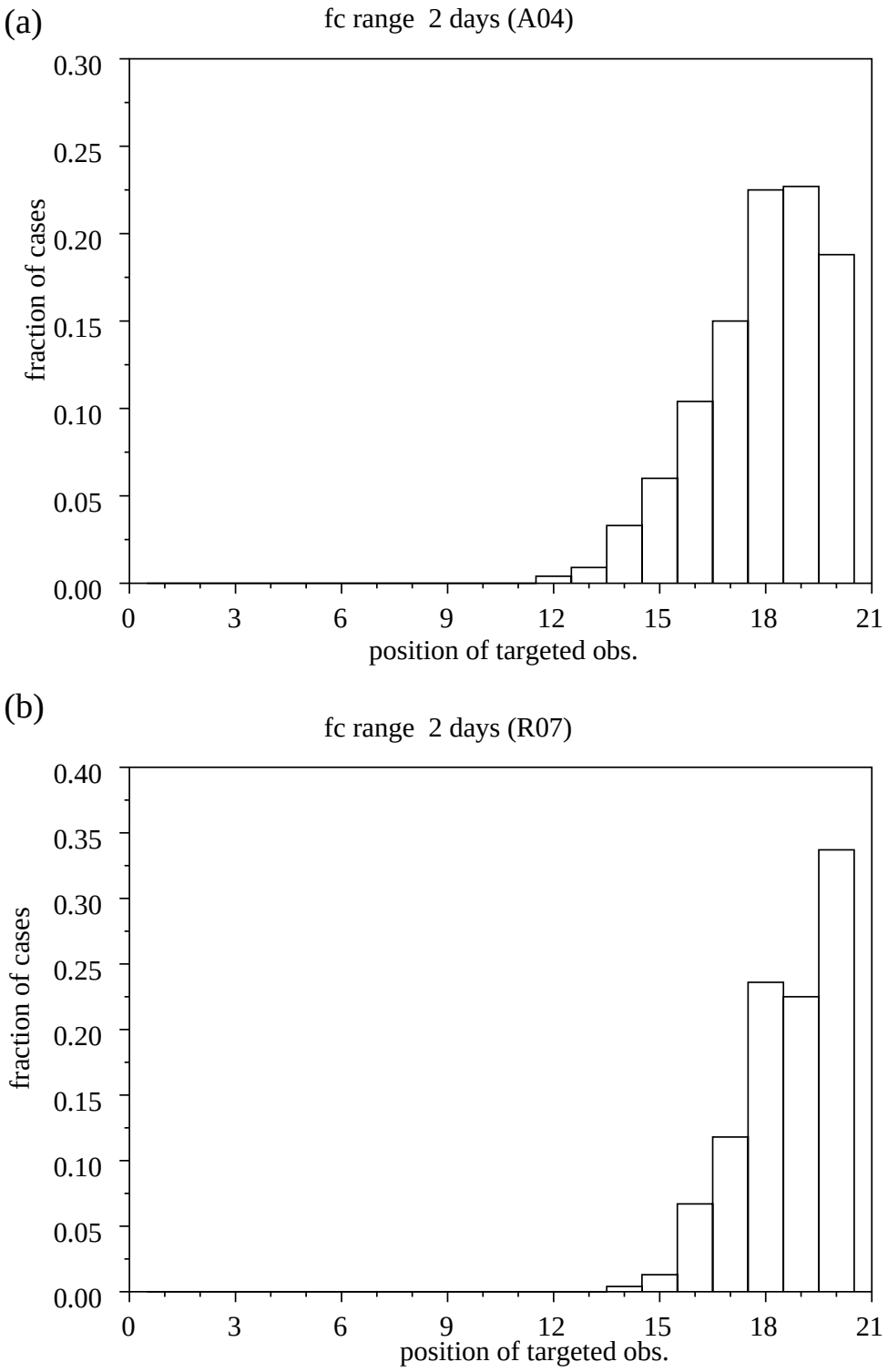


*Figure 8: Position of targeted observation sites using the KF for assimilation and targeting (a) and using OI for assimilation and OI-rank1 for targeting (b).*

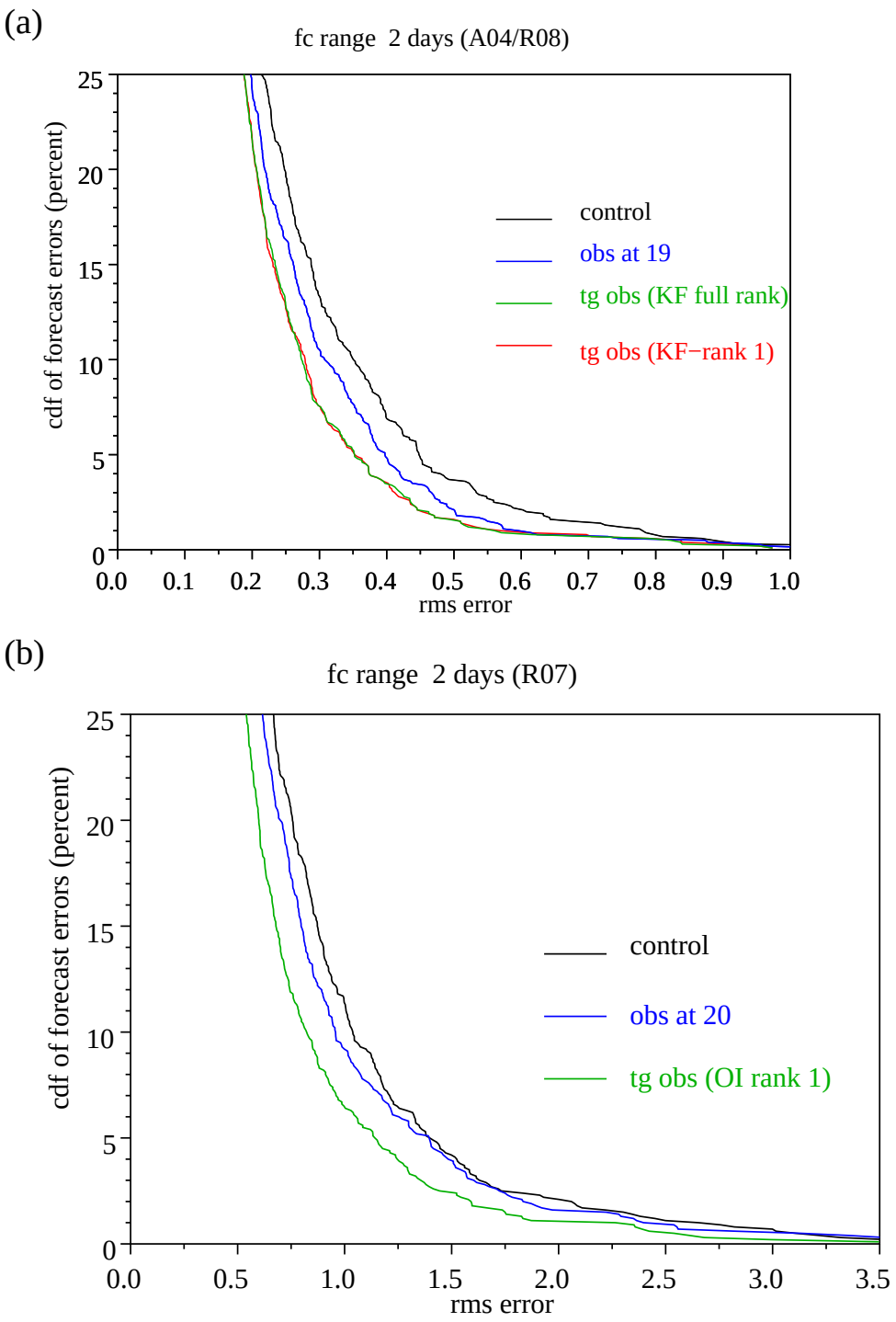


*Figure 9: Impact of adaptive observations on the 2-day forecast error distribution. Panel (a) KF assimilation and KF/KF-rank-1 targeting; panel (b) OI assimilation and OI-rank-1 targeting.*

applied in an operational NWP context. First, the implementation of a reduced rank estimate of forecast error variance based on an incremental variational assimilation scheme will be explained. Then, three examples will be given to illustrate the scope of this method.

### 4.1 Incremental Var and the Hessian reduced rank estimate

The ECMWF forecast system uses an incremental 4D-Var scheme. The analysis is found by minimising a cost function

$$J(\mathbf{x}) = \frac{1}{2}\mathbf{x}^{\mathrm{T}}\mathbf{B}^{-1}\mathbf{x} + \frac{1}{2}(\mathbf{H}\mathbf{x}-\mathbf{d})^{\mathrm{T}}\mathbf{R}^{-1}(\mathbf{H}\mathbf{x}-\mathbf{d}),$$

where the vector $\mathbf{x}$ denotes departure from the background and the vector $\mathbf{d}$ denotes departures of the observed values from the background interpolated to observations. The Hessian of the cost function of the variational assimilation scheme yields an estimate of the inverse of the analysis error covariance matrix.

$$\nabla\nabla J = \mathbf{B}^{-1} + \mathbf{H}^{\mathrm{T}}\mathbf{R}^{-1}\mathbf{H}$$

We assume here that $J$ is quadratic[11]. Therefore, the Hessian applied to an arbitrary vector can be computed exactly as finite difference of gradients.

Singular vectors computed with the routine Hessian[12] as initial time metric are used to define a reduced rank estimate of forecast error variance reductions. These vectors are referred to as Hessian singular vectors. Barkmeijer et al. (1998) introduced Hessian singular vectors and showed how they could be obtained from the iterative solution of a generalised eigenproblem. The reduced rank estimate of forecast error variance is defined as the variance of forecast errors projected into the subspace of routine Hessian singular vectors. Leutbecher (2003) introduced it and proposed the name Hessian reduced rank estimate. In order to quantify the effect of additional observations on the forecast error in the subspace of the routine Hessian singular vectors, it is necessary to compute the modified Hessian in the subspace of the leading $n$ routine Hessian singular vectors. Here, $n$ is the rank of the estimate. The modified Hessian in the subspace of the leading $n$ routine Hessian singular vectors is denoted by the $n$-by-$n$ matrix C. An efficient computation of this matrix is possible via

$$\begin{aligned} C_{ij} = \mathbf{v}_i^{\mathrm{T}}\nabla\nabla J_{\mathrm{mod}}\,\mathbf{v}_j &= \mathbf{v}_i^{\mathrm{T}}\left(\nabla\nabla J_{\mathrm{routine}} + \mathbf{H}_a^{\mathrm{T}}\mathbf{R}_a^{-1}\mathbf{H}_a\right)\mathbf{v}_j \\ &= \quad \delta_{ij} \;+\; (\mathbf{H}_a\mathbf{v}_i)^{\mathrm{T}}\,\mathbf{R}_a^{-1}\,\mathbf{H}_a\mathbf{v}_j. \end{aligned}$$

The main computational burden is the calculation of the routine Hessian singular vectors $\mathbf{v}_j$. To compute the matrix $\mathbf{C}$ it is sufficient to apply the observation operator for the additional observations $\mathbf{H}_a$ to each of the singular vectors. Then, the reduction of forecast error variance in the singular vector subspace is readily computed as

$$\mathrm{trace}\left(\left[\mathbf{I}-\mathbf{C}^{-1}\right]\mathrm{diag}(\sigma_1^2\ldots\sigma_{\mathrm{n}}^2)\right),$$

where the $\sigma_j$ denote the singular values of the routine Hessian singular vectors.

[11] This is the case for linearised observation operators. Note that the cost function used in the operational assimilation contains some non-quadratic terms, e.g. the one that represents variational quality control. The non-quadratic terms are neglected in the estimate of the analysis error covariance matrix used here.

[12] we use routine Hessian to refer to the metric associated with the routine observing network. Similarly, we will use modified Hessian to refer to the Hessian associated with the modified observing network consisting of the routine network and a set of additional observations.

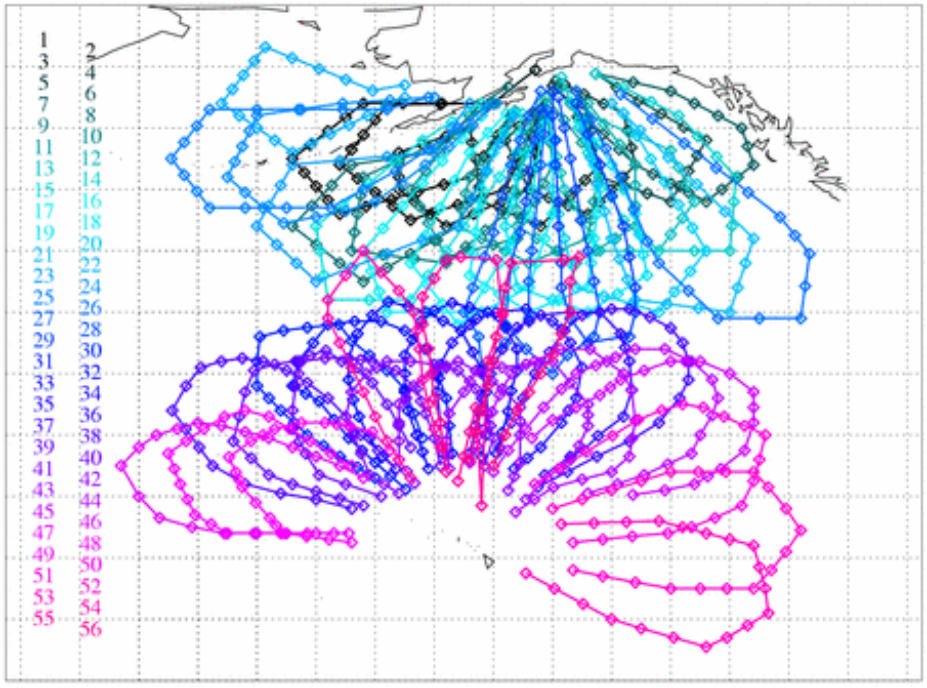

*Figure 10: Flight tracks considered during the Winter Storms Reconnaissance Program. Dots correspond to hypothetical dropsonde sounding locations.*

## 4.2 Ranking of flight tracks

The Hessian reduced rank estimate can be employed to select the best observing network upgrade among a finite number of feasible options. An example is the design of a flight track to deploy dropsondes over the ocean with the aim to improve a short-range forecast over the continent downstream. At NCEP, the Ensemble Transform Kalman filter is used operationally to select the best track for a targeting flight. Figure 11 shows an example of the predictions of forecast error variance reductions obtained with the Ensemble Transform Kalman filter and with the Hessian reduced rank estimate for a case during the last Winter Storms Reconnaissance Program.

The histogram provided by the Ensemble Transform Kalman filter is considerably flatter than the histogram obtained with the Hessian reduced rank estimate. Flights from Hawaii are generally expected to be more effective in reducing forecast error than those from Alaska according to the Hessian reduced rank estimate. In contrast, the Ensemble Transform Kalman filter shows little difference between the group of flight-tracks from Hawaii and the group from Alaska. However, the ordering of flight tracks obtained within each group is not too dissimilar for the two targeting techniques. The Atlantic TReC (2003) offers the opportunity for a more rigorous comparison between the Ensemble Transform Kalman filter and the Hessian Singular vectors.

## 4.3 Objective diagnosis of sensitive areas from singular vectors

Singular vectors have been used for observation targeting since the FASTEX experiment in 1997. Montani et al. (1999) and Buizza and Montani (1999) suggested to diagnose regions in which to place additional observations by means of a function defined as weighted average of the leading $n$ singular vectors. They proposed to use the singular values as weights to give more attention to those errors that contribute most to the forecast error in the verification region at verification time. Montani et al. (1999) based the function on temperature perturbations

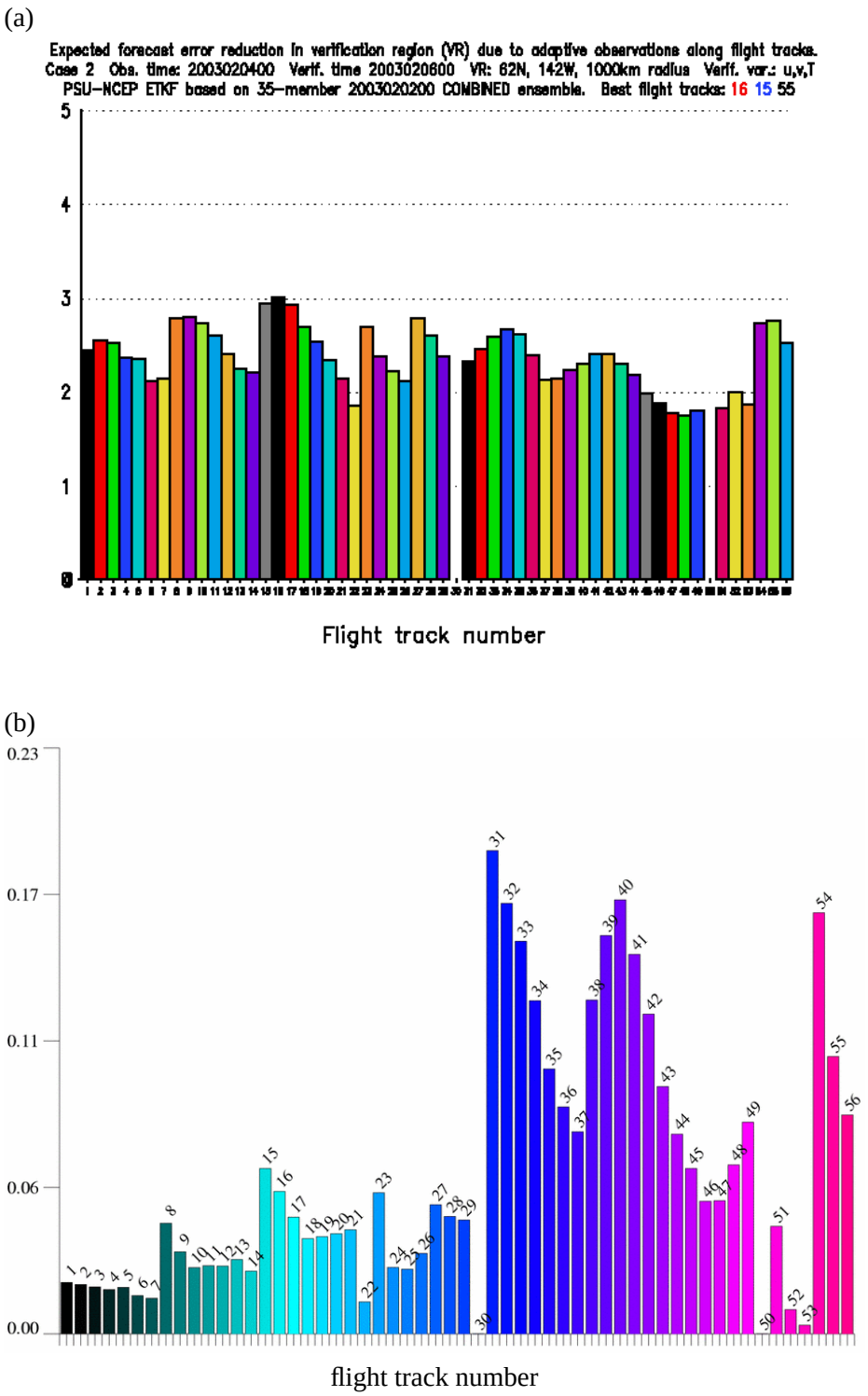


*Figure 11: Ranking of flight tracks using the Ensemble Transform Kalman Filter (a) and the Hessian reduced rank estimate (b). The value of each bar corresponds to the reduction of forecast error variance associated with a deployment of about 20 dropsondes along a flight track. The additional observations are aimed at improving the 48-hour forecast over Alaska, valid time: 6 Feb 2003, 0 UT, targeted observation time: 4 Feb 2003, 0 UT.*

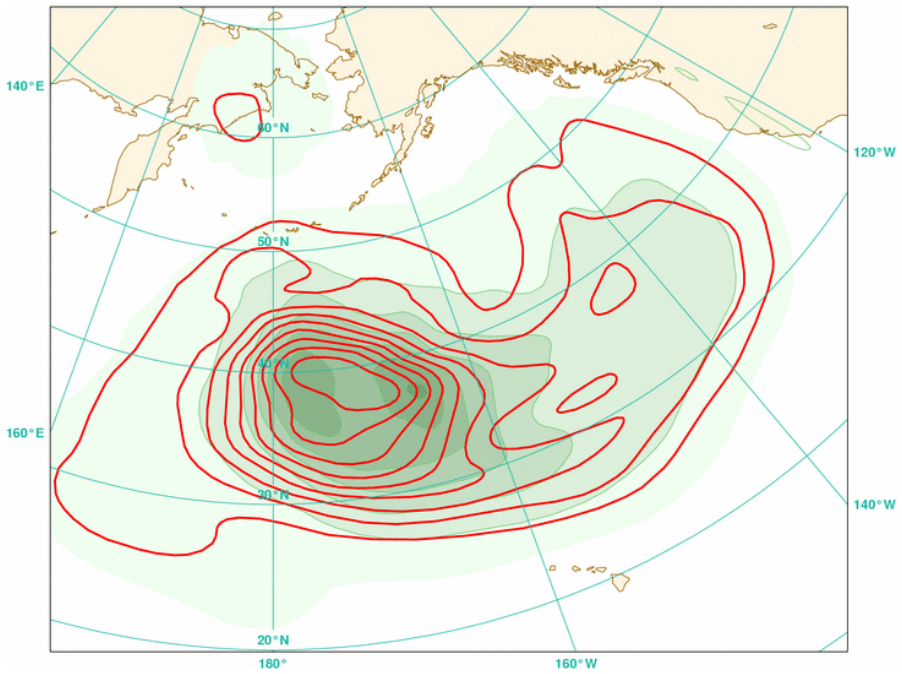


*Figure 12: Comparison of two ways to* objectively *diagnose a sensitive region from a set of leading singular vectors: The reduction of forecast error variance as function of the position of an additional dropsonde location is shaded; the function proposed by Buizza and Montani (1999), the singular-value-weighted average of the vertically integrated total energy, is contoured. Verification region over Alaska, 48-hour forecast range, observation time 4 Feb. 2003, 0 UT.*

of the singular vectors and Buizza and Montani (1999) based their function on the vertically integrated total energy of the singular vectors. Although this method allows to objectively diagnose a "sensitive" region from the singular vectors, a thorough theoretical justification for the choice of this diagnostic function has been lacking. With the Hessian reduced rank estimate this question can be addressed. Let us assume that we want to optimise the location of a couple of dropsondes. Then, the appropriate objective measure should be the forecast error variance reduction due to the use of an additional sounding at a given location. A plot of the forecast error variance reduction as function of the sounding location will indicate the region where the additional observation is likely to yield the largest forecast improvement. It turns out that the maps of forecast error variance reduction agree remarkably well with maps of the weighted average of the vertically integrated total energy of the singular vectors (Fig. 12). Thus, in retrospective the choice of the function by Buizza and Montani (1999) is justified.

### 4.4 Comparison of different observation types

Up to now, adaptive observation campaigns were focused on targeting in situ observations, predominantly dropsondes deployed from research aircraft over the oceans. In principle, one can apply targeting strategies to any kind of observation[13]. Furthermore, targeting techniques may become a tool for adaptive data selection strategies. These could help to cope with the huge stream of satellite data that will be available for NWP in a few years from now. In this context, the question arises whether the abundance of advanced satellite data will eliminate the need for targeted in situ observations. One may conjecture that adaptive in situ observations

[13] A first attempt to widen the scope of observation targeting is undertaken in the Atlantic THORPEX regional campaign Oct-Dec 2003, where additional soundings from ASAP ships, regular land stations and additional data from the AMDAR aircraft will be taken.

may still be useful to constrain the analysis below cloud where satellite observing capabilities are more limited. The Hessian reduced rank estimate can be employed to address that issue[14]. Forecast error variance reductions can be determined for different observation types such as targeted dropsondes and satellite radiances in the sensitive region and its surroundings. An example of such a comparison is presented in Fig. 13. The 20 dropsonde locations are selected to sample the target region well[15] whereas the HIRS data are not used in a cloudy region, which is associated with a front traversing the target region. In this case, the dropsondes are more efficient in constraining the forecast error over Europe at a range of 2 days than the HIRS radiances. However, the HIRS data may be important for constraining the error of subsequent analyses and forecasts by improving the first guess in the vicinity of the frontal zone. However, the presented methodology is not capable of quantifying improvements arising from an improved first guess field.

# 5 Discussion

Now, we will discuss the factors that are likely to affect the skill of the predictions of forecast error variance reductions for an operational NWP system.

## 5.1 Error dynamics

The estimates of forecast error variance are based on linear error dynamics. There are two issues here. First, we note that the tangent-linear model is not the tangent-linear of the nonlinear forecast model. The tangent-linear model and its adjoint are based on simplified version of the model — simplified in terms of the spatial resolution and in terms of the representation of parameterised physical processes[16]. Advances in the formulation of the tangent-linear and adjoint models should result in improved variance predictions. A test of the sensitivity of the observation targeting guidance to the spatial resolution and the representation of moist processes in the tangent-linear model will be performed during the Atlantic TReC[17]. Second, the validity of the tangent-linear assumption is a contentious issue. Gilmour et al. (2001) conclude that the tangent-linear assumption is probably not useful beyond 24 h. But their measure of nonlinearity is dominated by small scales. The results of Reynolds and Rosmond (2003) are more optimistic. They find that singular vectors can be useful at a range of up to 72 hours. Their diagnostic is similar to that of Gilmour et al. (2001) but the scale-dependence is studied explicitly. Furthermore, the diagnostic is applied in the space of the singular vectors.

## 5.2 Covariance estimates

The skill of the forecast error variance predictions depends on the quality of the background error covariance estimate. This has been illustrated by the comparison of the Kalman filter and OI experiments for the L95-system. Several presentations in this seminar deal with the estimation and representation of the background error covariances in data assimilation schemes[18]. Improvements in the covariance representation used in the

[14] different parts of the observing network are observing system experiments in which data from part of the network are denied. These experiments are computationally demanding as many assimilation cycles need to be run for each observing network configuration. The interpretation of individual cases is not very meaningful as results depend on the actual observation errors and background errors. The Hessian reduced rank estimate can be used to complement traditional observing system experiments. It has the advantage that it yields meaningful results for individual cases as it is a dynamic-statistical technique that provides expectation values rather than realizations.

[15] This is a hypothetical deployment.

[16] see presentation by Janiskova in this volume.

[17] Atlantic THORPEX Regional Campaign, Oct–Dec 2003.

[18] see, e.g., presentations by Fisher, Farrell and Ioannou, Houtekamer.

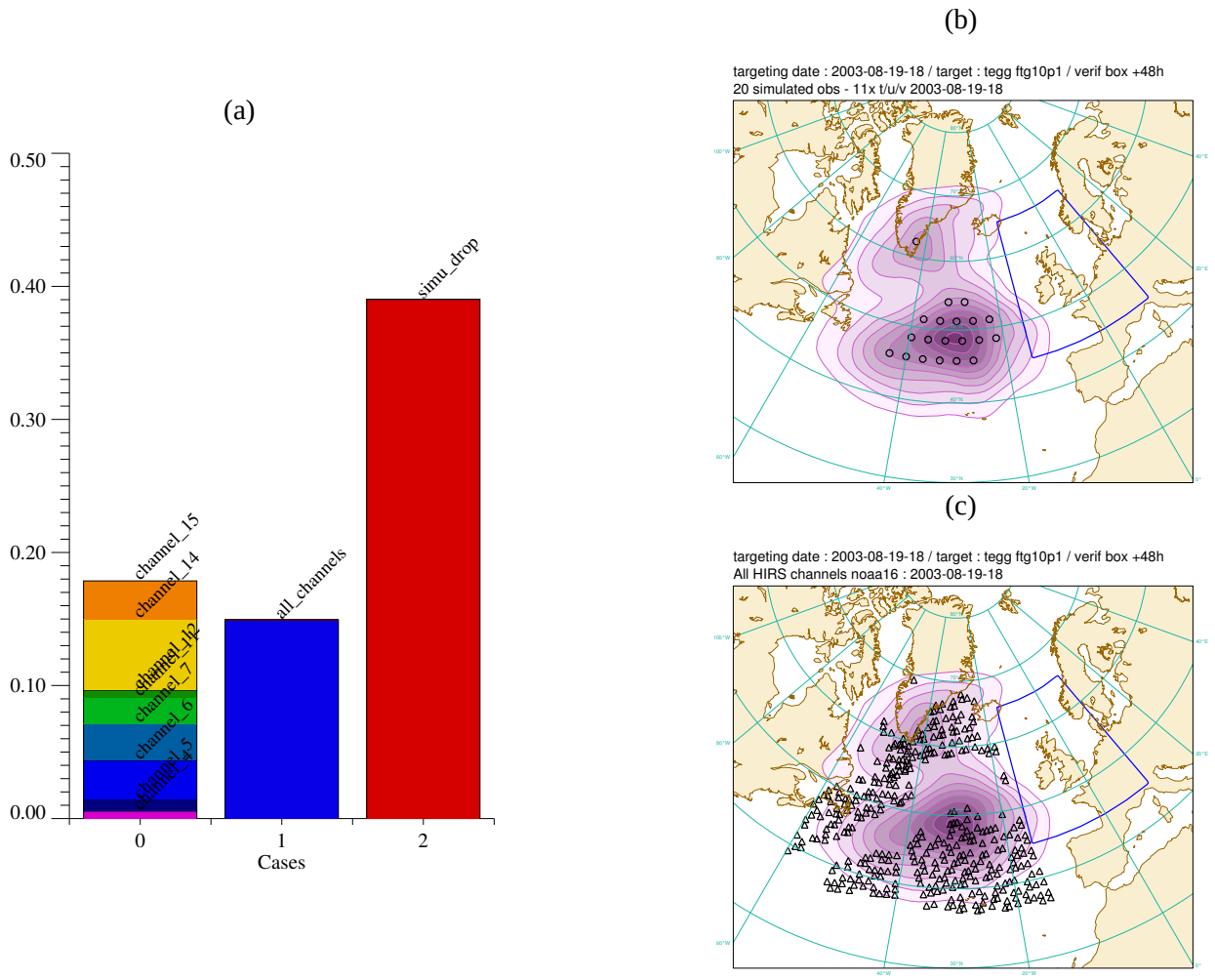


*Figure 13: Comparison of the reduction of forecast error variance (total energy in subspace of leading 10 singular vectors) due to 20 targeted dropsondes and due to HIRS radiances (a). The data coverage for the dropsondes and the radiances is plotted in panels (b) and (c), respectively. The shading in (b,c) is the sensitive region as diagnosed from the leading Hessian singular vectors.*

data assimilation are likely to be also beneficial for the associated targeting technique.

Correlated observation errors are largely unaccounted for in present assimilation schemes. Correlations of errors between channels and in space are expected for many satellite data, such as radiances and atmospheric motion vectors (Bormann et al. 2003). Predictions of forecast error variance reductions due to dense data with suspected error correlations should be interpreted with caution as long as these observation error correlations are not accounted for in the assimilation and targeting schemes. A possibility to address the problem without actually including correlated observation error in the assimilation scheme is optimal thinning of data Liu and Rabier (2002).

The targeting technique presented here faces one additional challenge that is not shared with the data assimilation schemes. It is necessary to predict the spatial distribution of used routine observations[19]. The spatial distribution of observations (and their error characteristics) have to be known before the observations are actually taken. For parts of the network, the day-to-day variability is small so that the latest available data coverage

[19] that is after the quality control steps.

provides a useful proxy for the coverage in the next few days. However, for satellite data affected by cloud it is a nontrivial task to predict the future data coverage. The relevance of this issue will grow with the amount and accuracy of satellite data used. It is conceivable that algorithms have to be developed that predict the data coverage based on forecast model cloud.

### 5.3 Rank Reduction

As the dimension of the singular vector subspace is increased the reduced rank estimate of forecast error variance converges to the prediction of forecast error variance that would be obtained with the Kalman filter. The question arises how many singular vectors are required to reliably predict the forecast error variance reductions. For the L95-system, one singular vector was sufficient. For the NWP problem, the answer will depend on the size of the verification region. A trivial upper bound for the dimension of the subspace is the number of degrees of freedom[20] in the verification region. A more useful bound can be obtained by looking at the fraction of forecast error explained by the $n$ leading singular vectors. Cardinali and Buizza (2003) find for 10 NORPEX cases that the leading 10 total energy singular vectors explain approximately 40% of the total forecast error in the verification region. Thus it appears that of the order of 10–100 singular vectors are required for a reliable prediction of forecast error variance reductions. In addition, there may be a necessity for updating the subspace in a sequential approach. Assume that already a part of the envisaged network upgrade constrains the error in the routine Hessian singular subspace well. Then, new singular vectors should be computed with the Hessian metric using the routine observations and the partial network upgrade in order to plan further adaptive observations. The necessity for such a sequential approach will depend on the size of the adaptable part of the observing network and on the dimension of the subspace

## 6 Conclusions

Adjoint-based tools to predict changes of forecast error variance due to modifications of the observing network have been discussed in this paper. The methods comprise the Kalman filter and approximations of it. The evaluation of these techniques was illustrated with experiments using the Lorenz 95 system. The rank-1 targeting technique based on the Kalman filter turned out to be as skilful as the full-rank Kalman filter. The rank-1 method that uses climatological background error covariances is also skilful. It is a targeting technique consistent with the used OI-assimilation. However, there appears a potential for improvements by accounting for flow-dependent aspects of the error statistics.

An objective for any targeting technique should be that it is based on analysis error covariance statistics which are consistent with the covariance estimates employed in the assimilation scheme which will use the adaptive observations. The Hessian reduced rank estimate is a targeting technique that achieves consistency with the 4D-Var assimilation scheme[21].

The verification of targeting techniques for operational NWP models, such as the Hessian reduced rank estimate, is a major outstanding task. Due to the statistical nature of the verification, large sample sizes are required. Data denial experiments may be better suited for the evaluation of targeting techniques than experiments with existing targeted observations for two reasons. The number of cases where targeted observations are available may be too small. Furthermore, for almost all of these cases deployments of additional observations outside the identified sensitive regions are lacking.

[20] number of grid points times number of variables. For a typical verification region with 2000 km horizontal extension and a T42 truncation for the singular vectors, this corresponds to about $6 \times 10^3$ degrees of freedom.

[21] to be precise: The inner loop of a 4D-Var scheme that uses a quadratic approximation of the cost function.

## Acknowledgements

I am grateful to Alexis Doerenbecher for providing the results presented in section 4 and useful comments on the manuscript. Thanks also to Erik Andersson for a suggestion that helped to improve the paper.

## References

Barkmeijer, J., M. Van Gijzen, and F. Bouttier, 1998: Singular vectors and estimates of the analysis-error covariance metric. *Quart. J. Roy. Meteor. Soc.*, **124**, 1695–1713.

Bergot, T. and A. Doerenbecher, 2002: A study on the optimization of the deployment of targeted observations using adjoint-based methods. *Quart. J. Roy. Meteor. Soc.*, **128**, 1689–1712.

Berliner, L. M., Z.-Q. Lu, and C. Snyder, 1999: Statistical design for adaptive weather observations. *J. Atmos. Sci.*, **56**, 2536–2552.

Bishop, C. H., B. J. Etherton, and S. J. Majumdar, 2001: Adaptive sampling with the ensemble transform Kalman filter. Part I: Theoretical aspects. *Mon. Wea. Rev.*, **129**, 420–436.

Bormann, N., S. Saarinen, G. Kelly, and J.-N. Thépaut, 2003: The spatial structure of observation errors in atmospheric motion vectors from geostationary satellite data. *Mon. Wea. Rev.*, **131**, 706–718.

Buizza, R. and A. Montani, 1999: Targeting observations using singular vectors. *J. Atmos. Sci.*, **56**, 2965–2985.

Cardinali, C. and R. Buizza, 2003: Forecast skill of targeted observations: A singular-vector-based diagnostic. *J. Atmos. Sci.*, **60**, 1927–1940.

Gilmour, I., L. A. Smith, and R. Buizza, 2001: On the duration of the linear regime: Is 24 hours a long time in weather forecasting? *J. Atmos. Sci.*, **58**, 3525–3539.

Hansen, J. A. and L. A. Smith, 2000: The role of operational constraints in selecting supplementary observations. *J. Atmos. Sci.*, **57**, 2859–2871.

Ide, K., P. Courtier, M. Ghil, and A. C. Lorenc, 1997: Unified notation for data assimilation: Operational, sequential and variational. *J. Meteor. Soc. Japan*, **75**(181–189).

Leutbecher, M., 2003: A reduced rank estimate of forecast error variance changes due to intermittent modifications of the observing network. *J. Atmos. Sci.*, **60**, 729–742.

Leutbecher, M., J. Barkmeijer, T. N. Palmer, and A. J. Thorpe, 2002: Potential improvement to forecasts of two severe storms using targeted observations. *Quart. J. Roy. Meteor. Soc.*, **128**, 1641–1670.

Liu, Z. and F. Rabier, 2002: The interaction between model resolution, observation resolution and observation density in data assimilation: A one-dimensional study. *Quart. J. Roy. Meteor. Soc.*, **128**, 1367–1386.

Lorenz, E. N., 1995: Predictability: A problem partly solved. In *Seminar on Predictability*, volume Vol. I, ECMWF, Reading, UK, 1–18.

Lorenz, E. N. and K. A. Emanuel, 1998: Optimal sites for supplementary weather observations: Simulation with a small model. *J. Atmos. Sci.*, **55**, 399–414.

Majumdar, S. J., C. H. Bishop, B. J. Etherton, I. Szunyogh, and Z. Toth, 2001: Can an Ensemble Transform Kalman Filter predict the reduction in forecast error variance produced by targeted observations? *Quart. J. Roy. Meteor. Soc.*, **127**, 2803–2820.

Montani, A., A. J. Thorpe, R. Buizza, and P. Unden, 1999: Forecast skill of the ECMWF model using targeted observations during FASTEX. *Quart. J. Roy. Meteor. Soc.*, **125**, 3219–3240.

Palmer, T. N., R. Gelaro, J. Barkmeijer, and R. Buizza, 1998: Singular vectors, metrics, and adaptive observations. *J. Atmos. Sci.*, **55**, 633–653.

Reynolds, C. A. and T. E. Rosmond, 2003: Nonlinear growth of singular-vector-based perturbations. *Quart. J. Roy. Meteor. Soc.*, **129**, 3059–3078.

Tippett, M. K., J. L. Anderson, C. H. Bishop, T. M. Hamill, and J. S. Whitaker, 2003: Ensemble square root filters. *Mon. Wea. Rev.*, **131**, 1485–1490.